Bioresource Technology 363 (2022) 127886

Contents lists available at ScienceDirect

Bioresource Technology

journal homepage: www.elsevier.com/locate/biortech

Directed reconstruction of a novel ancestral alcohol dehydrogenase featuring shifted pH-profile, enhanced thermostability and expanded substrate spectrum

Xiaoyu Chen [a], Zhe Dou [a], Tianwei Luo [a], Zewen Sun [a], Hongmin Ma [b], Guochao Xu [a,1,*], Ye Ni [a]

[a] Key laboratory of industrial Biotechnology, Ministry of Education, School of Biotechnology, Jiangnan University, Wuxi 214122, Jiangsu, China
[b] Key Laboratory of Combinatorial Biosynthesis and Drug Discovery, Ministry of Education and School of Pharmaceutical Sciences, Wuhan University, Wuhan 430072, China

HIGHLIGHTS

- An effective protocol for directed resurrection of ancestral enzymes.
- Ancestral ADH A64 was constructed with activity toward CPMK.
- A64 displays shifted pH profile, enhanced stability and expanded substrate spectrum.
- Shannon-Wiener index was used to describe the breadth of substrate spectrum of ancestral enzymes.

GRAPHICAL ABSTRACT

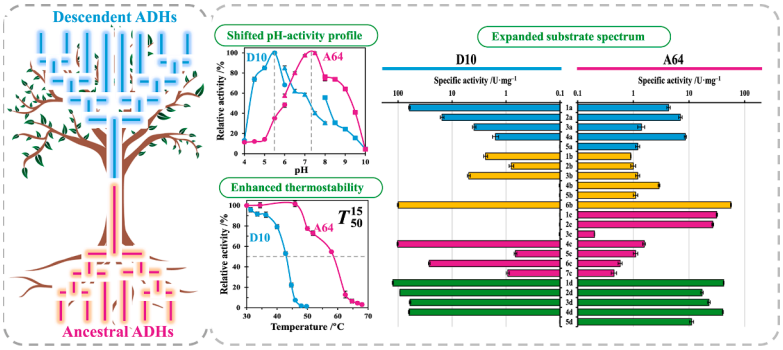

ARTICLE INFO

Keywords:
Alcohol dehydrogenase
Ancestral sequence reconstruction
pH-profile
Thermostability
Substrate spectrum

ABSTRACT

Ancestral enzymes are promising for industrial biotechnology due to high stability and catalytic promiscuity. An effective protocol was developed for the directed resurrection of ancestral enzymes. Employing genome mining with diaryl alcohol dehydrogenase *Kp*ADH as the probe, descendant enzymes D10 and D11 were firstly identified. Then through ancestral sequence reconstruction, A64 was resurrected with a specific activity of 4.3 $U \cdot mg^{-1}$. The optimum pH of A64 was 7.5, distinct from 5.5 of D10. The T15 50 and T_m values of A64 were 57.5 °C and 61.7 °C, significantly higher than those of the descendant counterpart. Substrate spectrum of A64 was quantitively characterized with a Shannon-Wiener index of 2.38, more expanded than D10, especially, towards bulky ketones in Group A and B. A64 also exhibited higher enantioselectivity. This study provides an effective protocol for constructing of ancestral enzymes and an efficient ancestral enzyme of industrial relevance for asymmetric synthesis of chiral alcohols.

* Corresponding author.
E-mail address: guochaoxu@jiangnan.edu.cn (G. Xu).
[1] ORCID: 0000-0001-9784-5648.

https://doi.org/10.1016/j.biortech.2022.127886
Received 23 July 2022; Received in revised form 27 August 2022; Accepted 29 August 2022
Available online 5 September 2022
0960-8524/© 2022 Elsevier Ltd. All rights reserved.

1. Introduction

Enzymes are increasingly regarded as the key chip or element for industrial biotechnology, especially in the context of emerging carbon neutral manufacture (Wang et al., 2021; Hu et al., 2021). In general, enzymes are manipulated to play a crucial role as biocatalysts or cell factories for an ever-expanding range of applications, including the efficient and sustainable production of value-added bioproducts such as fine chemicals, biofuels and natural products (Hollmann et al., 2020; Wu et al., 2020; Heath et al., 2021; Li et al., 2022). In the view of atomic economy and environmental friendliness, enzymes are of special interest for the synthesis of chiral secondary alcohols which have been widely applied as building blocks in pharmaceuticals, agrochemicals and food industries (Kang et al., 2019; Zerva et al., 2021). The sophisticated stereoselective structure renders enzymes high enantioselectivity and catalytic efficiency (Zheng and Xu, 2011). Therefore, enzymes can mitigate the use of toxic catalysts and the production of excessive chemical waste. However, currently, the application of enzymes is limited by poor operational stability and narrow substrate spectrum (Huisman et al., 2010; Bornscheuer et al., 2012; Bommarius and Paye, 2013). There is a constant need for discovering novel biocatalysts of industrial relevance with diverse properties, such as high thermostability, broad substrate scope and high enantioselectivity.

Tremendous attempts have been committed to mine naturally evolved enzymes or gear enzymes with enhanced stability and wide substrate spectrum (Wijma et al., 2013). Various strategies have been developed, such as traditional genome mining from thermophilic microorganisms (Zou et al., 2012), protein engineering based on consensus sequences (Jochens et al., 2010), directed evolution through random mutagenesis (Eijsink et al., 2005; Gumulya and Reetz, 2011), semi-rational engineering based on B-factor (Sun et al., 2019) etc. However, most of the methods are labor-intensive since the extant enzymes are specifically differentiated (Magliery et al., 2011). Moreover, there usually exists "trade-off" between stability and activity or enantioselectivity (Gong et al., 2016). Computational methods have also been applied to increase the stability (Korkegian et al., 2005; Romero et al., 2012), however, these depend on precise structure information and are usually resource-intensive. For most proteins, the information concerning sequence-structure–function relationships is insufficient to enable rational design (Pramanik et al., 2021). Moreover, it is difficult to predict epistatic effects during combinatorial process (Yu and Dalby, 2018). As a result, a general strategy for discovering enzymes with industrial relevance of both increased stability and wide substrate spectrum remains to be established.

Conceptually, modern enzymes are assumed to have evolved from a common ancestor, which should possess remarkable enzyme properties such as high stability and wide substrate spectrum. Ancestral sequence reconstruction (ASR) refers to the computational approximation based on phylogenetic tree of the extant protein sequences and statistical analysis using simple models of sequence evolution (Merkl and Sterner, 2016; Risso et al., 2018). ASR could be used in the resurrection of the ancestral enzymes (Ayuso-Fernández et al., 2017). Considering the large difference in terms of sequence and structure with descendant enzymes, ancestral enzymes are expected to display "unusual" or "extreme" properties (Spence et al., 2021). ASR has been successfully applied in the following aspects: (i) to identify novel P450 enzymes with diverse substrate profiles (Gumulya, et al., 2018); (ii) to stabilize 3-isopropylmalate dehydrogenase (Miyazaki et al., 2001); (iii) to enhance catalytic efficiency of cellulase (Barruetabeña et al.,2019); (iv) to modify substrate specificity of β-lactamase (Modi et al., 2021). Although ASR has been regarded as an efficient tool to explore evolutionary relationship between thermostability and catalytic promiscuity, the application of ASR in discovering of enzymes confronts the following issues: (i) the solubility of ancestral enzymes is usually poor (Rozi et al., 2022), (ii) the substrate spectrum and catalytic promiscuity lack quantitative characterization, (iii) the method for rational construction of ancestral enzymes with desired properties remains to be established.

To address the issues, a method was developed for directed resurrection of ancestral enzymes with desired properties. First, a traditional genome mining was performed to identify active descendant enzymes which display similar catalytic properties as the probe enzyme. Then, ancestral enzymes from the evolutional nodes of the active clans in the phylogenetic tree were resurrected and subjected to functional analysis to obtain active ancestral enzymes. The enzymatic properties of ancestral and descendant enzymes were characterized and compared in terms of pH-activity profile, temperature-activity profile, kinetic stability, thermostability, and biophysical stability. Furthermore, average activity and Shannon-Wiener index were introduced to quantitatively characterize the substrate spectrum and catalytic promiscuity of ancestral and descendant enzymes. The application potentials of ancestral enzymes in the asymmetric synthesis of chiral secondary alcohols were also evaluated. This study provides an effective protocol for directed resurrection of ancestral enzymes with desired properties and a robust and enantioselective ancestral enzyme of industrial relevance for the synthesis of bioproducts.

2. Material and methods

2.1. Chemical reagents, plasmid and strain

All prochiral ketones for analysis of substrate fingerprint were obtained from Aladdin Co. ltd. Cofactors NAD^+/NADH and $NADP^+$/NADPH were purchased from Bontac Bioengineering Co. ltd (Shenzhen, China). Other reagents were of analytic graded and purchased from Sinopharm Co. ltd (Shanghai, China). Expression vector pET28a and recombinant strain *E. coli* BL21(DE3) were previously constructed and stored in our lab.

2.2. Phylogenetic analysis and ancestral sequence reconstruction

Employing the amino acid sequence of *Kp*ADH as a probe, BLAST search was performed in Uniprot (https://www.uniprot.org/) and Protein Data Base (https://www.rcsb.org/) to retrieve the sequences with sequence identity of $>$ 30 %. After manually trimming the redundant sequences using CD-hit software, a total of 103 sequences were obtained. Alignment of all the sequences by ClustalW module in MEGA 6.0. Sequences with large gaps and too long length were further removed from the result in order to increase the fidelity of phylogenetic tree. The resultant 99 sequences were submitted to construct the phylogenetic tree using the maximum likelihood method and tested with bootstrap replications of 100 to increase the accuracy of the topology of phylogenetic tree. Employing the Jones-Taylor-Thornton model in FASTML web tool, ancestral sequences were predicted using Gamma Distribution statistic functions (Gumulya, et al., 2018).

2.3. Expression of descendant and ancestral alcohol dehydrogenases

All the genes coding for descendant and ancestral alcohol dehydrogenase genes were synthesized by Tianlin Biotechnol. Co. ltd (Wuxi, China) and were inserted into pET28a between restriction endonuclease sites of *Nde*I and *Xho*I. The recombinant plasmids were transferred into *E. coli* BL21(DE3) and verified by colony PCR and sequencing. ADHs were prepared by inoculating the positive recombinant strains in LB medium with 50 $\mu g \cdot mL^{-1}$ kanamycin and cultured at 37 °C and 180 rpm. Then 0.2 mM IPTG was supplemented into the culture when the OD_{600} reached 0.6–0.8 and further cultivated at 25 °C and 180 rpm for induction expression for 8 h. The cells were harvested by centrifuge at 8000 rpm and 4 °C for 10 min, washed three times with physiological saline, resuspended in PBS buffer (pH 7.0, 100 mM) and disrupted twice by high pressure homogenization at 800 bar under ice-water batch using ATS-BASICI (ATS Engineering Inc.). The crude enzyme extract was obtained by further centrifuge at 10000 rpm and 4 °C for 20 min, and

lyophilized under vacuum to obtain crude enzyme powder.

2.4. Protein purification of recombinant A64 and D10

Recombinant strains expressing genes of A64 and D10 were harvested, washed with physiological saline for two times and suspended in buffer A (20 mM PBS pH 7.4, 0.5 M NaCl), followed by disruption using high pressure homogenizer as above described. The resultant lysates were filtrated with 0.2 μm filter, and loaded onto a 1-mL crude Histrap FF column (GE Healthcare, Co. ltd, Shanghai, China), which was pre-equilibrated with buffer A. Crude extract of recombinant A64 and D10 were gradient eluted from the nickel column with imidazole concentrations increasing from 10 mM to 500 mM at a flow rate of 1 mL·min^{-1}. All the eluents were collected and submitted for SDS-PAGE analysis, and the eluents containing single bands were desalted against Tris-HCl buffer (pH 7.0, 100 mM) and concentrated at 3300 rpm and 4 °C. Purified A64 and D10 were stored at –80 °C for further characterization.

2.5. Activity assay

Standard protocol for activity assay of ADH was performed according to the changes in absorbance of NADPH at 340 nm (Xu et al., 2018). The reaction mixture consisted of 2 mM prochiral ketone dissolved in ethanol and 0.5 mM NADPH in 190 μL PBS buffer (pH 7.0, 100 mM), and 10 μL enzyme solution of appropriate concentrations at 30 °C. One unit of ADH activity was defined as the amount of ADH, under above conditions, required to catalyze the oxidation of 1 μmol NADPH per minute.

2.6. Enzyme characterization

Effects of pH and temperature on the activities of purified A64 and D10 were investigated with (4-chlorophenyl)(pyridin-2-yl)methanone (**1a**, CPMK) and 0.5 mM NADPH as substrates using the general activity assay protocol except in the following reaction buffers (100 mM): sodium citrate buffer (pH 4.0–6.0), PBS buffer (pH 6.0–8.0), glycine-NaOH buffer (pH 8.0–10.0) or at temperatures ranging from 25 °C to 70 °C (25, 30, 35, 40, 45, 50, 55, 60, 65 and 70 °C). All the assays were determined in triplicate.

Kinetic stability of purified A64 and D10 was determined by incubation of enzymes at different temperatures ranging from 30 °C to 70 °C for 15 min. Then, samples were submitted for activity determination using the general activity assay protocol. Thermostability of purified A64 and D10 at 40 °C and 50 °C was conducted by incubation of enzymes at 40 °C and 50 °C. At different time intervals, appropriate of samples were withdrawn from the incubation mixture to determine the residual activities employing the above-mentioned general activity assay protocol. Biophysical stability of purified A64 and D10 was determined using differential scanning calorimetry. Samples were heated from 20 °C to 95 °C, and the absorbance of protein was monitored accordingly. All the determinations were conducted for at least three times.

Effects of various metal ions including Fe^{3+}, Mg^{2+}, Co^{2+}, Cu^{2+}, Al^{3+}, Ag^{+}, Ni^{2+}, Mn^{2+}, Ca^{2+}, Zn^{2+} and EDTA on the activities of A64 and D10 were determined by incubation of each reagent at 1.0 mM with purified enzyme of 1 mg·mL^{-1} at 30 °C for 60 min. Control experiment was performed in the absence of any metal ions under the same conditions. The residual activity was determined using the above-mentioned standard protocol. All the assays were conducted for at least three times.

Kinetic parameters of purified A64 and D10 towards CPMK and NADPH were determined using the standard activity assay protocol except for at various substrate concentrations ranging from 0.1 mM to 10.0 mM for CPMK and 0.01 mM to 2.0 mM for NADPH. All the assays were conducted in triplicate. The apparent K_M, V_{max} and k_{cat} values were calculated according to the Lineweaver-Burk plot using double-substrates model.

2.7. Shannon-Wiener index analysis

The Shannon-Wiener index was adopted to describe the breadth of substrate spectrum of enzymes (Liu et al., 2013). Specific activities of purified A64 and D10 towards all the substrates in Group A-D were determined using the standard activity assay protocol for at least three times. The Shannon-Wiener index was calculated according to Eq. (1).

$$Shannon-Wiener\ index = -\sum_{i=1}^{n} Psi \times LnPsi,\ Psi = \frac{Asi}{A} \quad (1)$$

Where n is the number of all the tested substrates, A_{si} is the specific activity of enzyme towards a specific substrate of i (si), A is the sum of the specific activities towards all the tested prochiral ketones.

2.8. Conversion ratio and enantioselectivity analysis of A64 and D10

Reaction mixtures consisted of different concentrations of **1a** (100 mM), **5a** (10 mM), **1c** (100 mM), **1d** (100 mM), **4d** (100 mM), 1.5 equivalent of glucose, 10 U·mL^{-1} A64 or D10, 15 U·mL^{-1} GDH from *Bacillus subtilis*, 0.10 mM $NADP^{+}$ in 10 mL 100 mM PBS buffer (pH 7.5 for A64, pH 6.0 for D10). The reaction was performed at 30 °C and stirred at 120 rpm. The reaction pH was maintained by titration with 0.5 M NaOH. After reaction for 12 h, samples were withdrawn and extracted with equal volumes of ethyl acetate. The resultant organic phase was dried over anhydrous Na_2SO_4 and submitted for GC analysis equipped with CP-Chiralsil-Dex CB column to determine the conversion ratios and enantioselectivity (*e.e.* value) based on the analytical standards or previously reported methods (Xu et al., 2018).

3. Results and discussion

3.1. Directed resurrection of ancestral diaryl alcohol dehydrogenases

Phylogenetic tree of diaryl alcohol dehydrogenase *Kp*ADH, which exhibits high activity towards bulky-bulky ketones, and homologous proteins was constructed employing the maximum likelihood method and tested with bootstrap replications of 100 (Fig. 1). Ancestral enzymes were usually predicted from the nodes in the phylogenetic tree. Firstly, the ancestral ADH from the root node was designated as A1, which is generally regarded as the best ancestral ADH (Gumulya, et al., 2018). The sequence identity between A1 and *Kp*ADH was only 48.9 %. This ancestral ADH displays the largest evolutionary difference. However, recombinant A1 was expressed in insoluble form in *E. coli* BL21(DE3), according to the SDS-PAGE analysis, which might be attributed to the special and different folding types of ancestral enzymes. As expected, no activity was detected with recombinant A1. Hence, traditional resurrection of ancestral enzyme from root node is inscrutable and usually encountered with issues of insoluble expression.

To develop a method for directed resurrection of ancestral diaryl alcohol dehydrogenases, traditional genome mining was performed to identify active descendent ADHs with *Kp*ADH as probe sequence. As shown in Fig. 1, 16 potential ADHs from different evolutionary clans and with 30–70 % sequence identities of *Kp*ADH were selected and designated as D1-D16 for recombinant expression and examination in the asymmetric reduction of (4-chlorophenyl)(pyridin-2-yl)methanone (**1a**, CPMK). Most of the 16 potential ADHs could be expressed in soluble form in *E. coli* BL21(DE3). However, only putative ADH from *Kluyveromyces marxianus* under Genebank accession No. XP_022675166.1 and ADH from *Naumovozyma castellii* under Genebank accession No. XP_003673287.1, which were designated as D10 and D11 respectively, displayed activity towards **1a**. D10 and D11 share sequence identities of 47.3 % and 52.2 % with *Kp*ADH respectively. D10 is the most efficient in the reduction of **1a**, with specific activity of 61.6 U·mg^{-1} and *e.e.* of 97.1 % (*R*), much higher than 11.4 U·mg^{-1} and 82.0 % *e.e.* of *Kp*ADH (Table 1). D11 could catalyze the reduction of **1a**, with specific activity

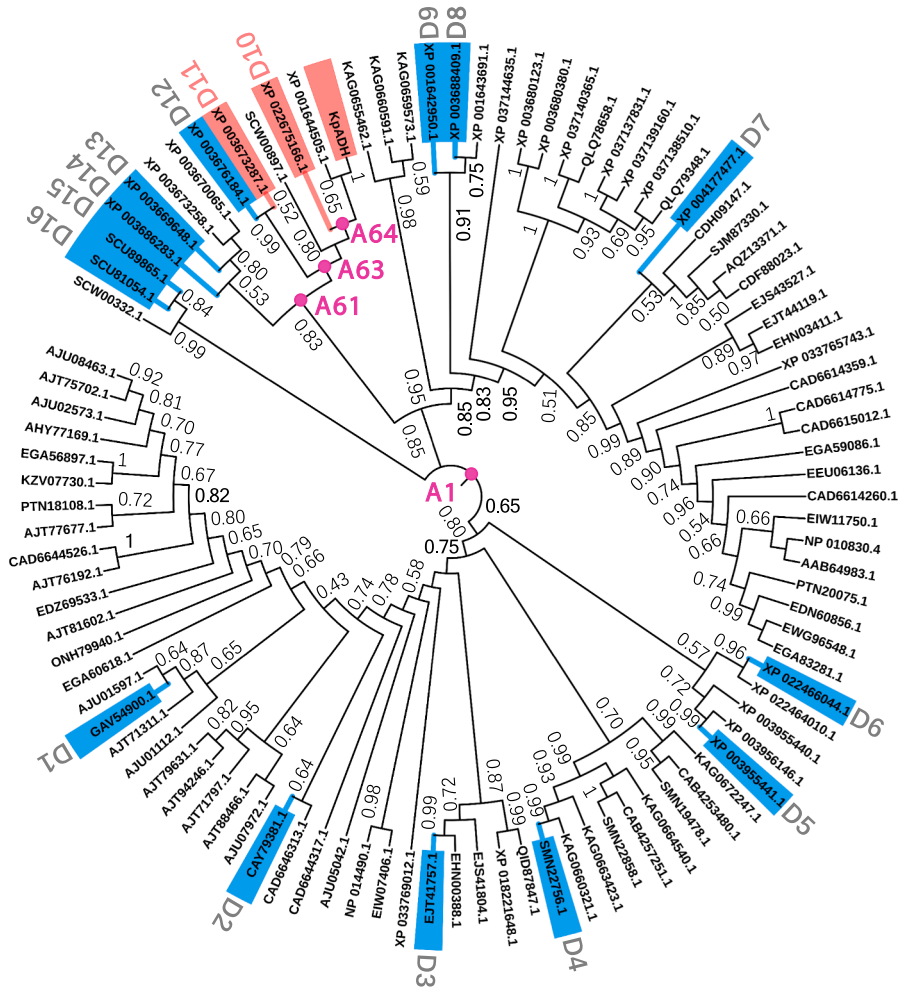

Fig. 1. Resurrection of ancestral ADHs employing ancestral sequence reconstruction strategy with *Kp*ADH as probe. Descendent ADHs for characterization were highlighted with different background color, blue: inactive ADH, red: active ADH. Ancestral ADH for characterization were illustrated with red dots. (For interpretation of the references to color in this figure legend, the reader is referred to the web version of this article.)

Table 1
Specific activity and enantioselectivity of descendant and ancestor ADHs towards CPMK.

Enzyme	Specific activity [U·mg^{-1}]	*e.e.* [%]/(*R*/*S*)
*Kp*ADH	11.4 ± 0.8	82.0 (*R*)
D10	61.6 ± 2.1	97.1 (*R*)
D11	2.0 ± 0.3	61.4 (*R*)
A61	1.5 ± 0.1	72.3 (*R*)
A64	4.3 ± 0.3	85.1 (*R*)

of 2.0 U·mg^{-1} and *e.e.* of 61.4 % (*R*).

Considering that enzymes from this evolutionary branch were active in the reduction of bulky-bulky ketones, ancestral ADHs from these evolutionary nodes, including A61, A63 and A64 with sequence identities of 66.3 %, 64.5 % and 71.8 % towards *Kp*ADH (Fig. 1), were evaluated for expression and reaction analysis. According to the SDS-PAGE analysis (Fig. 2), A61 and A64 were expressed in soluble form, while A63 was expressed as inclusion body. Activity and enantioselectivity analysis revealed that the specific activity and *e.e.* values of A61 and A64 were 1.5 U·mg^{-1} and 72.3 % (*R*), and, 4.3 U·mg^{-1} and 85.1 % (*R*). These results demonstrate that ancestral diaryl alcohol dehydrogenases were successfully and directedly resurrected from the active evolutionary clans. Although the specific activity and *e.e.* values were lower than the descendent *Kp*ADH and D10, the ancestral ADH might possess different enzyme properties of special interest for industrial biocatalysis. As a result, D10 and A64 were selected for further quantitative characterization of enzyme properties including pH-activity profile, temperature-activity profile, thermostability and catalytic promiscuity.

3.2. Enzyme characterization of A64 and D10

Ancestral ADH A64 and its descendent D10 belong to the "extended" short-chain dehydrogenase/reductase (SDR) subfamily based on the conserved motif analysis (Kallberg et al., 2002), although the sequence identity between them was merely 53.4 %. According to the multiple sequence alignment analysis, both A64 and D10 contain conserved motifs including SGxxGhxA motif (where × denotes any types of amino acids, h represents hydrophobic amino acids) in $\beta_1 + \alpha_1$ region for the binding of dinucleotide of coenzyme, DhxD in $\beta_3 + \alpha_3$ region for the binding of adenine ring of coenzyme, YxxSKxxhE in α_5 region for nucleophilic attack, etc (see supplementary materials) (Xu et al., 2018). The catalytic triads of A64 and D10 were Ser127-Tyr164-Lys168 and Ser127-Tyr165-Lys169, respectively. Similar catalytic motifs of A64 and D10 with SDR provide evidence for their common activity as alcohol dehydrogenases.

A64 consists of 345 aa with predicted molecular weight of 41.5 kDa,

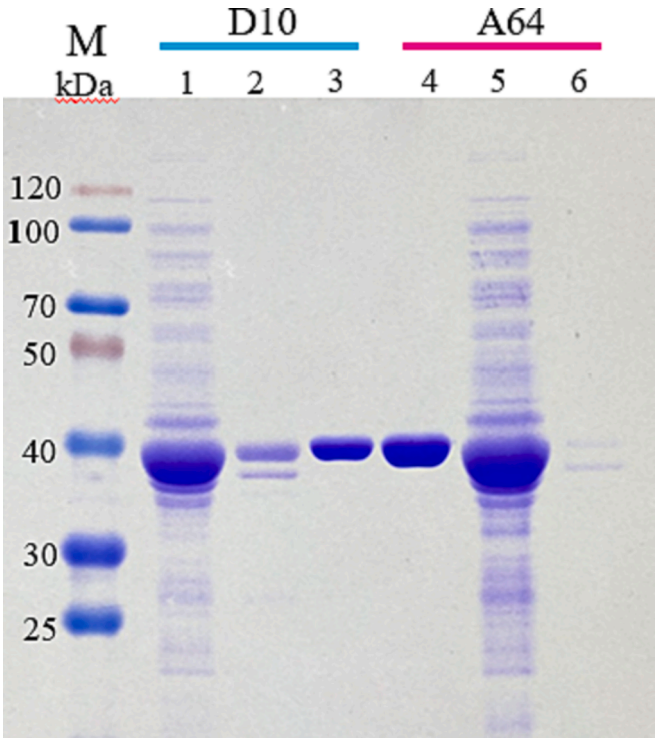

Fig. 2. SDS-PAGE analysis of the purified D10 and A64. Lane 1 & 2: supernatant and precipitant parts of D10; Lane 3: purified D10; Lane 5 & 6: supernatant and precipitant parts of A64; Lane 4: purified A64; Lane M: protein molecular marker.

while D10 is composed of 341 aa with predicted molecular weight of 40.4 kDa. After purification using nickel affinity chromatography, purified A64 and D10 migrated at around 40–45 kDa, consistent with their theoretical molecular weight (Fig. 2). Specific activity analysis revealed that both A64 and D10 prefer NADPH to NADH, which could be attributed to the DhxD motif. To further explore the difference in enzyme properties between ancestral and descendant ADHs, purified A64 and D10 were characterized in terms of pH-activity profile, temperature-activity profile, thermostability, and metal ions dependence.

Effect of pH values and buffer systems on the activities of A64 and D10 were investigated. As shown in Fig. 3**A, A64** exhibited different pH-activity profiles compared with D10. The optimum pH of A64 was determined to be pH 7.5, which is distinct from the optimum pH 5.5 of D10. The activities of A64 increased from pH 5.0 to pH 7.5, and decreased from pH 7.5 to pH 10.0. At pH 7.0 (PBS buffer), the relative activity of A64 is about 97.6 %, while the relative activity of D10 is about 58.7 %. The preference for basic conditions renders A64 a more promising biocatalyst than D10 since most of the cofactor regeneration systems are more efficient under basic conditions than acidic conditions, in addition to the higher stability of cofactor in basic conditions (Jia et al., 2022).

Effect of temperatures ranging from 25 °C to 70 °C on the activities of A64 and D10 were investigated as shown in Fig. 3**B**. A64 and D10 displays similar temperature-activity profiles, with optimum temperature of 40 °C. The activities of A64 increased from about 88 % at 25 °C to the highest activity at 40 °C, and then decreased along with the elevation of temperature. At 70 °C, the relative activity of A64 was 55.6 %, higher than 40.5 % of D10. Furthermore, thermostability of A64 and D10 was characterized in terms of kinetic stability (T15 50), thermostability (half-lives) and physical stability (T_m). The kinetic stability (T15 50) refers to the temperature at which the relative activity was 50 % after incubation for 15 min. According to Fig. 3**C**, the T15 50 value of A64 was 57.5 °C, about 15.1 °C higher than T15 50 of D10 (42.4 °C), indicating the significantly increased thermodynamic stability of the ancestral ADH. Then, the half-lives of A64 and D10 at 40 °C and 50 °C were also determined as illustrated in Fig. 3**D & 3E**. The half-lives of A64 at 40 °C and 50 °C were calculated to be about 27.5 h and 17.6 h respectively, about 29.9-fold and 352-fold of 0.92 h and 0.05 h of D10 at the same temperature. Therefore, ancestral enzyme A64 is much more stable than descendent D10. It is also well known that significant improvement in thermostability is hard to be achieved using laboratory-based evolution

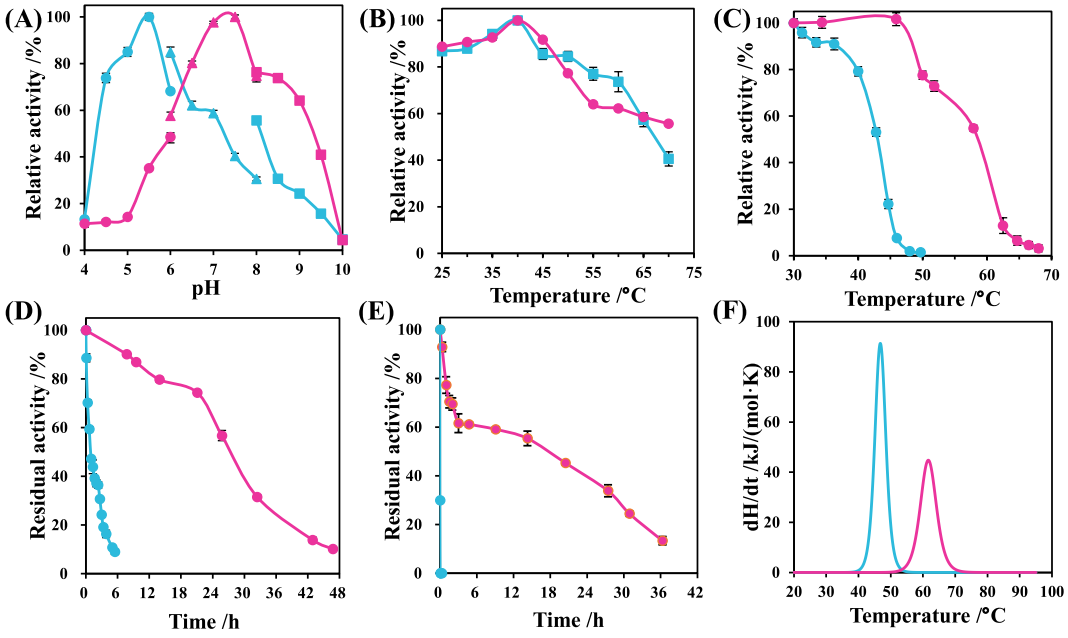

Fig. 3. Effect of pH and temperature on the activities of D10 and A64. (A) pH profiles, (B) temperature profiles, (C) *T*15 50 profiles, (D) residual activity at 40 °C, (E) residual activity at 50 °C, (F) T_m profiles. Blue: D10, red: A64. (For interpretation of the references to color in this figure legend, the reader is referred to the web version of this article.)

or protein engineering. Melting temperature (T_m), a biophysical parameter, refers to the temperature at which half of the tertiary or quaternary structures are destroyed, and reflects the structural rigidity of an enzyme. Employing differential scanning calorimetry, the T_m values of A64 and D10 were determined. As shown in Fig. 3**F**, the T_m and ΔH values of A64 were calculated to be 61.7 °C and 562 kJ·mol^{-1}, while the counterparts of D10 were 46.8 °C and 755 kJ·mol^{-1} respectively. The structure of A64 is more rigid than D10 and could resist high temperatures.

Metal ions dependence of A64 and D10 was also investigated by incubation of purified enzymes with different metal ions and EDTA (see supplementary materials). Under addition of 1 mM Al^{3+} and Mn^{2+}, the relative activities of A64 were 105 % and 102 % respectively. Cu^{2+} and Ag^{+} could significantly inhibit the activity of A64. The relative activity of A64 with EDTA was 92.4 %. Similar phenomenon was also found with D10. Taken together, ancestral and descendent ADHs identified in this study are not dependent on metal ions.

Based on above analysis, A64 is more promising than D10 in terms of optimum pH and stability. A64 displays significantly increased kinetic stability, thermostability and biophysical stability. To further explore the application potential of A64, the substrate specificity, kinetic parameters and enantioselectivity in the asymmetric reduction of prochiral ketones were investigated.

3.3. Substrate spectrum analysis of A64 and D10

Ancestral enzymes, possessing distinct structural differences from their extant counterparts, are generally regarded to have different substrate spectrum or catalytic promiscuity. However, these differences between ancestral and descendent ADHs are remain to be quantitively clarified. Previously, Shannon-Wiener index and average activity have been introduced to describe the “breadth” and “height” of substrate profiles of ADHs (Xu et al., 2018). Various prochiral ketones, including bulky-bulky ketones (Group A), bulky ketones (Group B), heterocyclic ketones and aliphatic ketones (Group C), aromatic and aliphatic ketone esters (Group D), were selected to characterize the substrate spectrum of

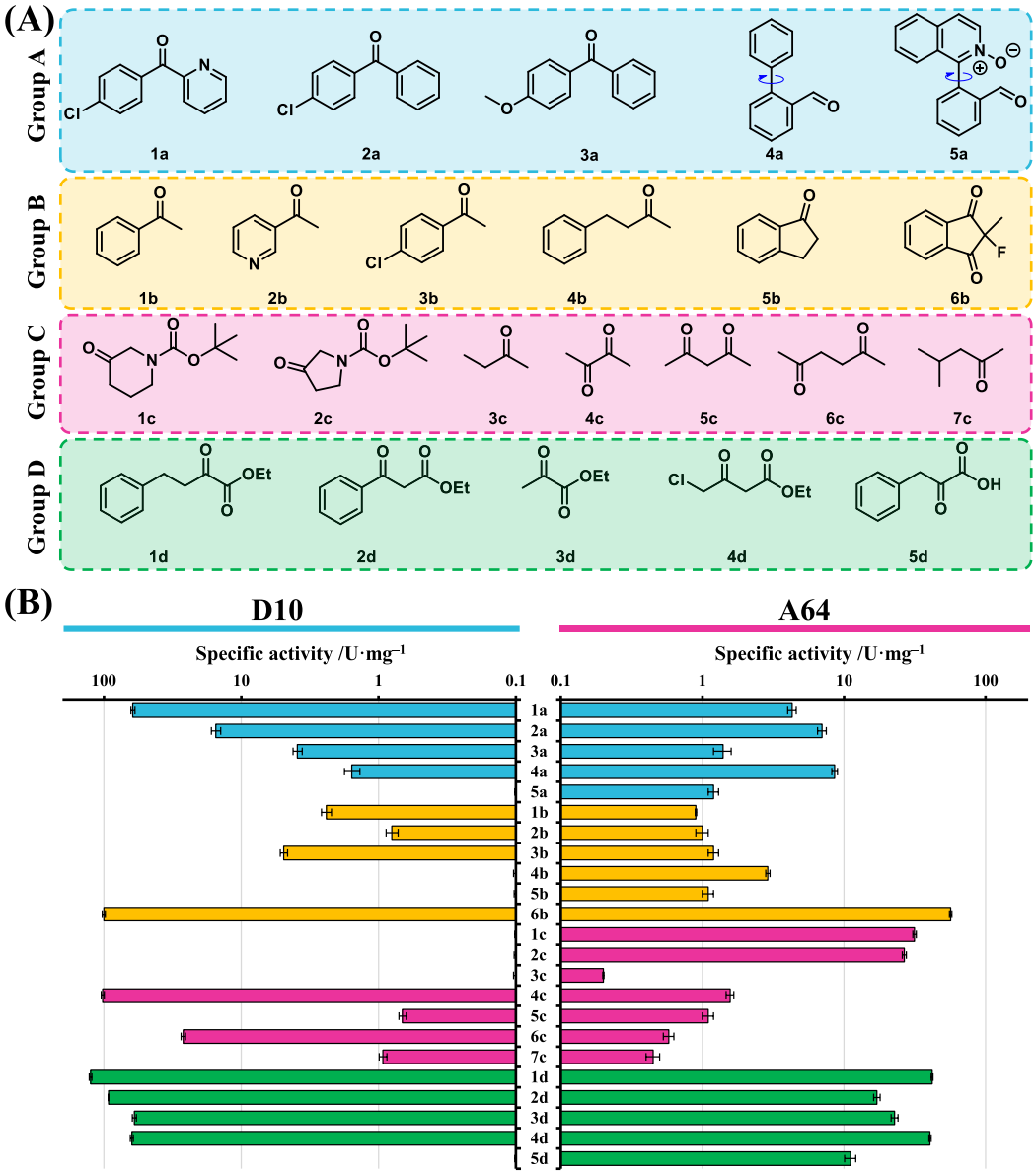

Fig. 4. Substrates applied for the characterization of ADHs (A) and the substrate fingerprints of purified D10 and A64 (B). (■): Group A, (■): Group B, (■): Group C, (■): Group D.

ancestral and descendent ADHs (Fig. 4**A**). Specific activities of A64 and D10 towards all the prochiral ketones were determined and illustrated in Fig. 4**B**. A64 could catalyze the reduction of all the tested ketones, while D10 could only reduce parts of substrates. Nevertheless, the average activity of D10 towards all the tested substrates was 28.8 U·mg^{-1}, 2.34-fold of 12.3 U·mg^{-1} of A64. The highest activity of D10 was 125 U·mg^{-1} towards ethyl 2-oxo-4-phenylbutanoate (1d), while the highest activity of A64 was detected towards 2-fluoro-2-methyl-1*H*-indene-1,3(2H)-dione (6b) with specific activity of 56.7 U·mg^{-1}. Taken together, descendent ADH D10 has higher catalytic efficiency than ancestral ADH A64. However, the Shannon-Wiener index of D10 towards all the tested substrates was 2.18, lower than 2.38 of A64 (Table 2), demonstrating that A64 has wider substrate spectrum and higher catalytic promiscuity.

Furthermore, the detailed difference between A64 and D10 in average activity and Shannon-Wiener index towards substrates of each group was analyzed (Table 2). For the ketones with bulky-bulky substituents in Group A, the average activity of A64 was about 4.5 U·mg^{-1}, only 27.3 % of 16.5 U·mg^{-1} of D10. However, the Shannon-Wiener index of A64 towards Group A was 1.37, about 1.79-fold of D10. This indicates that, after natural evolution and selection, extant enzymes become more specific, namely, with narrowed substrate spectrum. The ancestral enzymes, *vice versa*, exhibit higher catalytic promiscuity except for the compromised catalytic efficiency. For aromatic ketones in Group B, the average activity of A64 was 10.6 U·mg^{-1}, significantly lower than 18.5 U·mg^{-1} of D10, while the Shannon-Wiener index of A64 was 0.51, much higher than 0.35 of D10, demonstrating that A64 exhibits broader substrate spectrum and lower catalytic efficiency than D10 towards aromatic ketones. Similar trend was also found towards cyclic and aliphatic ketones in Group C. The average activity of A64 was 10.3 U·mg^{-1}, only 47.7 % of 21.6 U·mg^{-1} of D10. The Shannon-Wiener index of A64 was 0.97, 1.64-fold of 0.59 of D10. With regard to the ketoesters or ketoacid in Group D, both A64 and D10 displayed high catalytic efficiency. The average activity of A64 was 26.7 U·mg^{-1} towards substrates in Group D, significantly higher than substrates in Group A-C, while the average activity of D10 towards substrates in Group D was as high as 68.0 U·mg^{-1}, indicating that both A64 and D10 displayed preference for ketoesters. The Shannon-Wiener index of A64 towards substrates in Group D was 1.50, 11.9 % higher than 1.34 of D10. In addition, Shannon-Wiener index towards substrates in Group D of both A64 and D10 was higher than that of Group A-C. These results demonstrate that ancestral enzyme A64 displays expanded substrate spectrum and higher catalytic promiscuity in terms of Shannon-Wiener index, despite of compromised catalytic efficiency.

The kinetic parameters of A64 and D10 towards CPMK and NADPH were also determined. As shown in Table 3, the K_M and k_{cat} values of D10 towards CPMK were 0.39 mM and 17.5 s^{-1} respectively, with k_{cat}/K_M of 44.9 s^{-1}·mM^{-1}, while K_M and k_{cat} values of A64 were 3.59 mM and 3.93 s^{-1} with k_{cat}/K_M of 0.68 s^{-1}·mM^{-1}. Compared with the extant counterpart, ancestral enzyme A64 displayed lower substrate binding affinity and catalytic efficiency, which could be attributed to the increased catalytic specificity along with the evolution. However, the K_M value towards NADPH of A64 was as low as 0.08 mM, significantly lower than 0.31 mM of D10, hinting that ancestral enzyme A64 has higher binding affinity for NADPH, which might better adapt to specific ancient environment with insufficient cofactors. In summary, ancestral enzyme A64 possesses relatively high cofactor binding affinity, however, low substrate binding affinity and catalytic efficiency.

Table 2
Comparison of substrate fingerprint characterization parameters of D10 and A64.

Entry		D10	A64
Best substrate		**1d**	**6b**
Highest activity /U·mg^{-1}		125 ± 2.7	56.7 ± 1.1
Average activity /U·mg^{-1}		28.8	12.3
Shannon-Wiener index		2.18	2.38
Group A	Average activity /U·mg^{-1}	16.5	4.5
	Shannon-Wiener index	0.76	1.37
Group B	Average activity /U·mg^{-1}	18.1	10.6
	Shannon-Wiener index	0.35	0.51
Group C	Average activity /U·mg^{-1}	21.6	10.3
	Shannon-Wiener index	0.59	0.97
Group D	Average activity /U·mg^{-1}	68.0	26.7
	Shannon-Wiener index	1.34	1.50

Table 3
Kinetic parameters of D10 and A64 towards CPMK and NADPH.

Enzyme	Substrate	K_M [mM]	k_{cat} [s^{-1}]	k_{cat}/K_M [s^{-1}·mM^{-1}]
D10	CPMK	0.39 ± 0.05	17.5 ± 1.49	44.9
	NADPH	0.31 ± 0.03	59.2 ± 0.03	191
A64	CPMK	3.59 ± 0.51	3.93 ± 1.36	0.68
	NADPH	0.08 ± 0.01	12.6 ± 0.3	158

3.4. Asymmetric reduction of prochiral ketones using A64 and D10

Industrial biocatalysis has been increasingly accepted as "first-of-choice" in the synthesis of value-added bioproducts, due to its high efficiency, high enantioselectivity and mild reaction conditions. Hence, as a promising biocatalyst with industrial relevance, enzymes should possess high stability, wide substrate spectrum, and high enantioselectivity. The ancestral ADH A64 identified in this study displayed better stability and wider substrate spectrum than its extant counterpart. To further explore its application potential in industrial biosynthesis, the capacity of this ancestral ADH in the asymmetric reduction of prochiral ketones was evaluated. Since A64 is NADPH-dependent, glucose dehydrogenase from *Bacillus subtilis* with relatively high activity towards NADPH was introduced for cofactor regeneration (Xu et al., 2018).

Substrates that A64 exhibited relatively high activity in each Group were selected to evaluate its application potential, including **5a**, **6b**, **1c**, **1d**, **4d** (Table 4). Substrate **5a**, a bulky-bulky ketone with axial chirality, is generally regarded as "hard-to-reduce" by enzymes. A64 could catalyze the asymmetric reduction of 10 mM **5a** within 12 h, with conversion ratio of > 99.9 % and *e.e.* value of 78.1 % (*R*), while D10 could not catalyze the reduction of **5a**. To the best of our knowledge, this is the first report on the biocatalytic reduction of prochiral biaryl aldehydes/ketones using recombinant alcohol dehydrogenases. Ancestral ADH A64 not only exhibits relatively high activity but also atroposelectivity in the reduction of biaryl substrates. Substrate **6b** is also a near-symmetry substrate, and could be reduced by dynamic kinetic resolution. Both A64 and D10 displayed high activity towards **6b**, and could catalyze the complete conversion of as high as 100 mM **6b** into alcohols, with > 99.9 % conversion ratio within 12 h. However, the absolute configuration and the *e.e.* value of product remain to be clarified, due to the lack of analytical standard. Substrate **1c** is a heterocyclic ketone, and its corresponding alcohol is the key building block of antitumor drug Ibrutinib, one of the top selling pharmaceuticals (Zheng et al., 2017). A64 could also catalyze the complete reduction of as high as 100 mM **1c**, producing (*S*)-alcohol in 99.0 % *e.e.*. Ketoesters **1d** and **4d** from Group D are

Table 4
Conversion and enantioselectivity of D10 and A64 towards prochiral ketones.

Substrate [a]	D10		A64	
	Conv. [%]	*e.e.* [%]	Conv. [%]	*e.e.* [%]
5a	<0.1	–	>99.9	78.1 (*R*)
6b	>99.9	*n. a.* [b]	>99.9	*n. a.*.
1c	<0.1	–	>99.9	99.0 (*S*)
1d	>99.9	96.0 (*R*)	>99.9	99.2 (*R*)
4d	>99.9	99.9 (*S*)	>99.9	99.9 (*S*)

[a] substrate concentration: 10 mM **5a**, 100 mM **6b**, 100 mM **1c**, 100 mM **1d**, 100 mM **4d**.
[b] *n. a.* denotes not available.

important starting materials for the synthesis of ethyl (*R*)-2-hydroxy-4-phenylbutanoate and ethyl (*S*)-3-hydroxy-4-chlorobutanoate respectively, which are important building blocks for angiotensin converting enzyme inhibitors drugs and cholesterol-lowering drug Atorvastatin (Xu et al., 2018). Both A64 and D10 could catalyze the asymmetric reduction of **1d** and **4d**. The *e.e.* value of A64 towards **1d** was 99.2 % (*R*), higher than 96.0 % (*R*) of D10. Substrate **4d** (100 mM) could be fully converted by A64 and D10 with 99.9 % *e.e.* (*S*). As a result, this ancestral enzyme A64 could be applied in the asymmetric reduction of prochiral ketones for the synthesis of chiral alcohols with high enantioselectivity. Various chiral secondary alcohols would be synthesized employing this resurrected ancestral enzyme according to the results of substrate spectrum analysis.

4. Conclusions

In this study, a strategy was developed for directed resurrection of ancestral alcohol dehydrogenases with desired catalytic properties. Employing diaryl alcohol dehydrogenase *Kp*ADH as a probe, two novel descendant enzymes D10 and D11 were identified with high activity towards CPMK. Furthermore, active ancestral enzyme A64 was resurrected from the evolutionary node of D10 and *Kp*ADH. A64 displays a shifted pH-activity profile, significantly increased thermostability, wider substrate spectrum and higher catalytic promiscuity than D10. This study provides an effective protocol for directed resurrection of active ancestral enzymes, and a promising biocatalyst with industrial relevance for the synthesis of value-added chiral alcohols.

Availability of data and materials.

All data generated or analyzed during this study are included in this published article and its supplementary information files.

Funding.

We are grateful to the National Key Research and Development Program (2019YFA0906400), the National Natural Science Foundation of China (22078127), Open Funding Project of the Key laboratory of industrial Biotechnology (KLIB-KF202101) and Program of Introducing Talents of Discipline to Universities (111–2-06) for the financial support of this research.

Ethical statement This article does not contain any studies with human participants or animals performed by any of the authors.

CRediT authorship contribution statement

Xiaoyu Chen: Investigation, Data curation, Writing – original draft, Validation. **Zhe Dou:** Formal analysis. **Tianwei Luo:** Formal analysis. **Zewen Sun:** Formal analysis. **Hongmin Ma:** Conceptualization. **Guochao Xu:** Methodology, Conceptualization, Writing – review & editing, Supervision, Funding acquisition. **Ye Ni:** Conceptualization, Supervision, Funding acquisition, Writing – review & editing.

Declaration of Competing Interest

The authors declare that they have no known competing financial interests or personal relationships that could have appeared to influence the work reported in this paper.

Data availability

Data will be made available on request.

Appendix A. Supplementary data

Supplementary data to this article can be found online at https://doi.org/10.1016/j.biortech.2022.127886.

References

Ayuso-Fernández, I., Martínez, A. T., Ruiz-Duenas, F. J. 2017. Experimental recreation of the evolution of lignin-degrading enzymes from the Jurassic to data. Biotechnol. Biofuels. 10, 67. (https://doi.org/10.1186/s13068-017-0744-x).

Barruetabeña, N., Alonso-Lerma, B., Galera-Prat, A., Joudeh, N., Barandiaran, L., Aldazabal, L., Arbulu, M., Alcalde, M., De Sancho, D., Gavira, J.A., Carrion-Vazquez, M., Perez-Jimenez, R., 2019. Resurrection of efficient Precambrian endoglucanases for lignocellulosic biomass hydrolysis. Commun. Chem. 2, 76. (https://doi.org/10.1038/s42004-019-0176-6).

Bommarius, A. S., Paye, M. F. 2013. Stabilizing biocatalysts. Chem. Soc. Rev. 42, 6534-6565. (https://doi.org/10.1039/c3cs60137d).

Bornscheuer, U. T., Huisman, G. W., Kazlauskas, R. J., Lutz, S., Moore, J. C., Robins, K. 2012. Engineering the third wave of biocatalysis. *Nature*, 485, 185-194. (https://doi.org/10.1038/nature11117).

Eijsink, V. G. H., Gaseidnes, S., Borchert, T. V., van den Bur, B. 2005. Directed evolution of enzyme stability. Biomol. Eng. 22, 21-30. (https://doi.org/10.1016/j.bioeng.2004.12.003).

Gong, Y., Xu, G. C., Chen, Q., Yin, J. G., Li, C. X., Xu, J. H. 2016. Iterative multitarget evolution dramatically enhances the enantioselectivity and catalytic efficiency of *Bacillus subtilis* esterase towards bulky benzoate esters of DL-menthol. Catal. Sci. Technol. 6, 2370-2376. (https://doi.org/10.1039/c5cy01723h).

Gumulya, Y., Reetz, M. T. 2011. Enhancing the thermal robustness of an enzyme by directed evolution: least favorable starting points and inferior mutants can map superior evolutionary pathways. ChemBioChem 12, 2502-2510. (https://doi.org/10.1002/cbic.201100412).

Gumulya, Y., Baek, J. M., Wun, S. J., Thomson, R. E. S., Harris, K. L., Hunter, D. J. B., Behrendorff, J. B. Y. H., Kulig, J., Zheng, S., Wu, X. M., Wu, B., Stok, J., de Voss, J. J., Schenk, G., Jurva, U., Andersson, S., Isin, E. M., Bodén, M., Guddat, L., Gillam, E. M. J. 2018. Engineering highly functional thermostable proteins using ancestral sequence reconstruction. Nat. Catal. 1, 878-888. (https://doi.org/10.1038/s41929-018-0159-5).

Heath, R. S., Ruscoe, R. E., Turner, N. J. 2021. The beauty of biocatalysis: sustainable synthesis of ingredients in cosmetics. Nat. Prod. Rep. 39, 335-388. (https://doi.org/10.1039/d1np00027f).

Hollmann, F., Opperman, D. J., Paul, C. E. 2020. Biocatalytic reduction reactions from a Chemist's perspective. Angew. Chem. Int. Ed. 60, 5644-5665. (https://doi.org/10.1002/anie.202001876).

Hu, G. P., Li, Z. H., Ma, D. L., Ye, C., Zhang, L. P., Gao, C., Liu, L. M., Chen, X. L. 2021. Light-driven CO_2 sequestration in *Escherichia coli* to achieve theoretical yield of chemicals. Nat. Catal. 4, 395-406. (https://doi.org/10.1038/s41929-021-00606-0).

Huisman, G. W., Liang, J., Krebber, A. 2010. Practical chiral alcohol manufacture using ketoreductases. Curr. Opin. Chem. Biol. 14, 122-129. (https://doi.org/10.1016/j.cbpa.2009.12.003).

Jia, Q., Zheng, Y. C., Li, H. P., Qian, X. L., Zhang, Z. J., Xu, J. H. 2022. Engineering isopropanol dehydrogenase for efficient regeneration of nicotinamide cofactors. Appl. Environ. Microbiol. 88, 15. (https://doi.org/10.1128/aem.00341-22).

Jochens, H., Aerts, D., Bornscheuer, U. T. 2010. Thermostabilization of an esterase by alignment-guided focused directed evolution. Protein Eng. Des. Sel. 23, 903-909. (https://doi.org/10.1093/protein/gzq071).

Kallberg, Y., Oppermann, U., Jörnvall, H., Persson, B. 2002. Short-chain dehydrogenase/reductases (SDRs) Coenzyme-based functional assignments in complete genomes. Eur. J. Biochem. 269, 4409-4417. (https://doi.org/10.1046/j.1432-1033.2002.03130.x).

Kang, X. M., Cai, X., Liu, Z. Q., Zheng, Y. G. 2019. Identification and characterization of an amidase from *Leclercia adecarboxylata* for efficient biosynthesis of L-phosphinothricin. Bioresour. Technol. 289, 121658. (https://doi.org/10.1016/j.biortech.2019.121658).

Korkegian, A., Black, M. E., Baker, D., Stoddard, B. L. 2005. Computational thermostabilization of an enzyme. Science 309 857-860. (https://doi.org/10.1002/9783527815128.ch7).

Li, Q., Ma, C. L., Di, J. H., Ni, J. C., He, Y. C. 2022. Catalytic valorization of biomass for furfuryl alcohol by novel deep eutectic solvent-silica chemocatalyst and newly constructed reductase biocatalyst. Bioresour. Technol. 2022, 347, 126376. (https://doi.org/10.1016/j.biortech.2021.126376).

Liu, J.Y., Zheng, G.W., Li, C.X., Yu, H.L., Pan, J., Xu, J.H., 2013. Multi-substrate finger printing of esterolytic enzymes with a group of acetylated alcohols and statistic analysis of substrate spectrum. J. Mol. Catal. B: Enzym. 89, 41–47. (https://doi.org/10.1016/j.molcatb.2012.12.008.).

Magliery, T. J., Lavinder, J. J., Sullivan, B. J. 2011. Protein stability by number: high-throughput and statistical approaches to one of protein science's most difficult problems. Curr. Opin. Chem. Biol. 15, 443-451. (https://doi.org/10.1016/j.cbpa.2011.03.015).

Merkl, R., Sterner, R. 2016, Ancestral protein reconstruction: techniques and applications. Biol. Chem. 397, 1-21. (https://doi.org/10.1515/hsz-2015-0158).

Miyazaki, J., Nakaya, S., Suzuki, T., Tamakoshi, M., Oshima, T., Yamagishi, A. 2001. Ancestral residues stabilizing 3-isopropylmalate dehydrogenase of an extreme thermophile: experimental evidence supporting the thermophilic common ancestor hypothesis. J. Biochem. 129, 777-782. (https://doi.org/10.1093/oxfordjournals.jbchem.a002919).

Modi, T., Risso, V. A., Martinez-Rodriguez, S., Gavira, J. A., Mebrat, M. D., van Horn, W. D., Sanchez-Ruiz, J. M., Banu Ozkan, S. 2021. Hinge-shift mechanism as a protein design principle for the evolution of β-lactamases from substrate promiscuity to specificity. Nat. Commun. 12, 1852. (https://doi.org/10.1038/s41467-021-22089-0).

Pramanik, S., Contreras, F., Davari, M. D., Schwaneberg, U. 2021. Protein engineering by efficient sequence space exploration through combination of directed evolution and computational design methodologies. Protein Eng. 153-176. (https://doi.org/10.1002/9783527815128).

Risso, V. A., Sanchez-Ruiz, J. M., Ozkan, S. B., 2018, Biotechnological and protein-engineering implications of ancestral protein resurrection. Curr. Opin. Struct. Biol. 51, 106-115. (https://doi.org/10.1016/j.sbi.2018.02.007).

Romero, P. A., Stone, E., Lamb, C., Chantranupong, L., Krause, A., Miklos, A., Hughes, R. A., Fechtel, B., Ellington, A. D., Arnold, F. H., Georgiou, G. 2012. SCHEMA-designed variants of human arginase I & II reveal sequence elements important to stability and catalysis. ACS Synth. Biol. 1, 221-228. (https://doi.org/10.1021/sb300014t).

Rozi, M. F. A. M., Abd Rahman, R. N. Z. R., Leow, A. T. C., Ali, M. S. M. 2022. Ancestral sequence reconstruction of ancient lipase from family I.3 bacterial lipolytic enzymes. Mol. Phylogenet. Evol. 168, 107381. (https://doi.org/10.1016/j.ympev.2021.107381).

Spence, M. A., Kaczmarski, J. A., Saunders, J. W., Jackson, C. J. 2021. Ancestral sequence reconstruction for protein engineers. Curr. Opin. Struct. Biol. 69, 131-141. (https://doi.org/10.1016/j.sbi.2021.04.001).

Sun, Z. T., Liu, Q., Qu, G., Feng, Y., Reetz, M. T. 2019. Utility of B-factors in protein science: interpreting rigidity, flexibility, and internal motion and engineering thermostability. Chem. Rev. 119, 1626-1665. (https://doi.org/10.1021/acs.chemrev.8b00290).

Wang, Z., Sundara Sekar, B., Li, Z., 2021. Recent advances in artificial enzyme cascades for the production of value-added chemicals. Bioresource Technology 323, 124551.

Wijma, H.J., Floor, R. J., Janssen, D.B. 2013. Structure- and sequence-analysis inspired engineering of proteins for enhanced thermostability. Curr. Opin. Struc. Biol. 23, 588-594. (https://doi.org/10.1016/j.sbi.2013.04.008).

Wu, S. K., Snajdrova, R., Moore, J. C., Baldenius, K., Bornscheuer, U. T. 2020, Biocatalysis: Enzymatic synthesis for industrial applications. Angew. Chem. Int. Ed. 60, 88-119. (https://doi.org/10.1002/anie.202006648).

Xu, G. C., Zhang, Y. P., Wang, Y., Ni, Y. 2018. Genome hunting of carbonyl reductases from *Candida glabrata* for efficient preparation of chiral secondary alcohols. Bioresour. Technol. 247, 553-560. (https://doi.org/10.1016/j.biortech.2017.09.111).

Yu, H. R., Dalby, P. A. 2018. Coupled molecular dynamics mediate long- and short-range epistasis between mutations that affect stability and aggregation kinetics. Proc. Natl. Aca. Sci. USA 115, E11043-E11052. (https://doi.org/10.1073/pnas.1810324115).

Zerva, A., Pentari, C., Ferousi, C., Nikolaivits, E., Karnaouri, A. Topakas, E. 2021. Recent advances on key enzymatic activities for the utilization of lignocellulosic biomass. Bioresour. Technol. 342, 126058. (https://doi.org/10.1016/j.biortech.2021.126058).

Zheng, G. W., Xu, J. H. 2011 New opportunities for biocatalysis: driving the synthesis of chiral chemicals. Curr. Opin. Biotechnol. 22, 784-792. (https://doi.org/10.1016/j.copbio.2011.07.002).

Zheng, G. W., Liu, Y. Y., Chen, Q., Huang, L., Yu, H. L., Lou, W. Y., Li, C. X., Bai, Y. P., Li, A. T., Xu, J. H. 2017. Preparation of structurally diverse chiral alcohols by engineering ketoreductase CgKR1. ACS Catal. 7, 7174-7181. (https://doi.org/10.1021/acscatal.7b01933).

Zou, Z. Z., Yu, H. L., Li, C. X., Zhou, X. W., Hayashi, C., Sun, J., Liu, B. H., Imanaka, T., Xu, J. H. 2012. A new thermostable beta-glucosidase mined from *Dictyoglomus thermophilum*: Properties and performance in octyl glucoside synthesis at high temperatures. Bioresour. Technol. 118, 425-430. (https://doi.org/10.1016/j.biortech.2012.04.040).